Available online at www.sciencedirect.com

ScienceDirect

Transportation Research Procedia 00 (2018) 000–000

Transportation Research Procedia

www.elsevier.com/locate/procedia

World Conference on Transport Research - WCTR 2019 Mumbai 26-31 May 2019

A simulation study on optimizing the pattern of speed reduction markings affecting speed choice before curve entry

Hirofumi Yotsutsuji[a]*, Toshimori Otazawa[b], Hideyuki Kita[b]

[a] *CERI, PWRI, 1-3-1-34 Hiragishi, Toyohira-ku, Sapporo, Hokkaido 062-8602, Japan*
[b] *Kobe University, 1-1 Rokkodai, Nada-ku, Kobe, Hyogo 657-8501, Japan*

Abstract

Speed reduction markings (SRMs) on road surfaces are consisting of transverse marking lines with decreasing spacing in the direction of vehicle movement. The driver of a leading vehicle moving on SRM-installed lane toward a curve is exposed to accident risk due to shortage of deceleration and rear-end collision of a following vehicle. To avoid such risk, the decreasing spacing pattern of the marking lines needs to be optimized according to a speed trajectory of the leading vehicle. The aim of this study is to examine the optimal pattern by simulating both the vehicle speed trajectory and the rear-end collision, constructing an optimal control model of driving behavior with speed perception and combining it with a car-following model. In the case of SRMs before the sharp bend, our numerical examples showed the results as follows: 1) The spacing pattern in which a decreasing rate of the spacing is greater in the end section than in the remaining sections may produce a high risk of the rear-end collision, although the leading vehicle safely enters the curve. 2) The spacing pattern in which the decreasing rate is zero in all sections may produce an accident with which the leading driver meets within the curve, although the rear-end collision risk is very few. These results indicate that optimizing the pattern of SRMs affecting speed choice of the leading driver entry must consider not only the vehicle speed trajectory of the leading vehicle but also the rear-end collision risk of the following vehicle.

Peer-review under responsibility of WORLD CONFERENCE ON TRANSPORT RESEARCH SOCIETY.

Keywords: Speed reduction markings ; Pattern Design ; Driver perception ; Dynamic optimization ; MCMC estimation ; Rear-end collision risk

1. Introduction

Speed reduction markings (SRMs) on road surfaces are transverse marking lines with decreasing spacing in the direction of vehicle movement. When SRMs are installed on a straight lane adjacent to a transition curve section, it is expected that SRMs encourage drivers to reduce their vehicle speed safely before they enter the curve. The Manual on

* Corresponding author. Tel.: +81-11-841-1738; fax: +81-11-841-9747.
E-mail address: yotsutsuji-h@ceri.go.jp

Peer-review under responsibility of WORLD CONFERENCE ON TRANSPORT RESEARCH SOCIETY

Uniform Traffic Control Devices, MUTCD (FHWA, 2009) explains that the effect of speed reduction by SRMs is caused by a pattern of progressively reduced spacing to give the drivers the impression that their speed is increasing. However, MUTCD does not explain the optimal spacing pattern of SRMs installed before the curve. The driver of a leading vehicle moving on SRM-installed lane toward the curve may be exposed to accident risk due to shortage of deceleration and rear-end collision of a following vehicle. MUTCD does not explain sufficient conditions for preventing such risk. To avoid such risk, the spacing pattern of SRMs needs to be optimized according to a speed trajectory of the leading vehicle approaching the curve.

The aim of this study is to examine the optimal spacing pattern of SRMs affecting the leading driver's speed choice before the curve entry by simulating both the speed trajectory of the leading vehicle and the rear-end collision of the following vehicle. To achieve this aim, we construct an optimal control model of driving behavior with speed perception, which is based on Pontryagin's maximum principle, and combine it with a car-following model to evaluate a rear-end collision risk index called PICUD.

The body of this paper consists of seven chapters. Chapter 2 describes two mathematical models. One is a model regarding perception and behavior of the leading driver, and the other is a model of car-following behavior to evaluate PICUD. Chapter 3 describes how to solve the optimal control problem regarding the perception and behavior of the leading driver and how to estimate the model parameters. Chapter 4 describes details of simulation data obtained from a driving simulation experiment that has already been conducted in our previous study. Chapters 5, 6 and 7 describe simulation results, discussion and conclusion, respectively.

2. Modeling

2.1. Perception and behavior of a leading driver

We impose the following two assumptions on modeling speed perception and driving behavior of a driver of the leading vehicle traveling on SRM-installed lane toward the curve.

Firstly, concerning the speed perception, we assume that the driver can recognize the maximum value of vehicle speed at which the vehicle can safely pass through the curve, even though the driver did not know the actual value. We set the maximum safe speed which the driver recognizes before entering the curve and that at which the vehicle passes through the curve as $\hat{v}_{\mathrm{S}}$ and $\hat{v}_{\mathrm{O}}$, respectively. Hereafter, subjective and objective values are denoted by suffixes "S" and "O", respectively, at the lower-right corner of each variable. The important points are that these speeds are independent with respect to time t, and that SRMs cannot affect these speeds at all. We also assume that the driver can perceive the vehicle speed on SRM-installed lane at time t, without watching a speedometer of the vehicle. We set the vehicle speed which the driver perceives at time t and the actual vehicle speed at time t as $v_{\mathrm{S}}(t)$ and $v_{\mathrm{O}}(t)$, respectively. The important points are that a discrepancy may occur between $v_{\mathrm{S}}(t)$ and $v_{\mathrm{O}}(t)$ when the driver does not watch the speedometer, and that $v_{\mathrm{S}}(t)$ can only be affected by the spacing pattern of SRMs through visual speed perception of the driver. For the model simplification, we assume that the derivative of the vehicle speed with respect to time t, $\dot{v}_{\mathrm{O}}(t)$, is proportional to the derivative of the perceived speed with respect to time t, $\dot{v}_{\mathrm{S}}(t)$. When $v_{\mathrm{O}}(t)$ exceeds $\hat{v}_{\mathrm{O}}$ (or $\hat{v}_{\mathrm{S}}$), speeding accidents may occur within the curve.

Secondly, concerning the driving behavior, we assume that the driver can choose the vehicle speed to maximize a utility defined by $v_{\mathrm{S}}(t)$ under condition of $\hat{v}_{\mathrm{S}}$. We set this utility as $U(v_{\mathrm{S}}(t)|\hat{v}_{\mathrm{S}})$, which is referred to as "speed utility" in this study. We also assume that, at the beginning location of SRM-installed lane, the driver can draw out a plan to enter the curve safely by use of dynamic optimization technique (Chiang, 1992). Then, the driver can maximize the sum of present discounted value of $U(v_{\mathrm{S}}(t)|\hat{v}_{\mathrm{S}})$ that the driver will obtain at every step on SRM-installed lane in order to enter the curve at the optimal vehicle speed. The driver operates the vehicle toward the curve in accordance with this plan in a rational manner.

Under the above-mentioned assumptions, the optimal control problem that the driver should solve between at time $t = 0$ at the beginning location and at time $t = T$ at the end location of SRM-installed lane can be formulated as follows:

$$\underset{v_{\mathrm{S}}(0),\cdots,v_{\mathrm{S}}(T)}{\mathrm{Maximize}} \int_0^T U(v_{\mathrm{S}}(t)|\hat{v}_{\mathrm{S}}) \exp[-\sigma t]\,\mathrm{d}t, \tag{1}$$

$$\text{subject to} \quad f(v_{\mathrm{O}}(t), L(t)) = v_{\mathrm{S}}(t) + \dot{v}_{\mathrm{S}}(t), \tag{2}$$

$$\dot{v}_{\mathrm{S}}(t) = \alpha \dot{v}_{\mathrm{O}}(t), \tag{3}$$

$$f(v_{\mathrm{O}}(t), L(t)) = \left\{1 + L(t)^{-\xi}\right\} v_{\mathrm{O}}(t), \tag{4}$$

$$v_{\mathrm{O}}(0) = \bar{v}_{\mathrm{O}} > 0, \tag{5}$$

$$v_{\mathrm{O}}(T) \exp[-\bar{\sigma} T] \geq 0, \tag{6}$$

$$U(v_{\mathrm{S}}(t) | \hat{v}_{\mathrm{S}}) = \mu v_{\mathrm{S}}(t) - \exp[\mu\{v_{\mathrm{S}}(t) - \hat{v}_{\mathrm{S}}\}], \tag{7}$$

where,
$v_{\mathrm{S}}(t)$: instantaneous speed perceived by the leading driver at time t,
$v_{\mathrm{O}}(t)$: instantaneous speed of the leading vehicle at time t,
$\hat{v}_{\mathrm{S}}$: maximum safe speed recognized by the leading driver,
$L(t)$: line interval of SRMs at time t,
$\dot{v}_{\mathrm{S}}(t)$: derivative of $v_{\mathrm{S}}(t)$ with respect to time t,
$\dot{v}_{\mathrm{O}}(t)$: derivative of $v_{\mathrm{O}}(t)$ with respect to time t,
σ : discount rate of time preference,
α, ξ : parameters,
μ : degree of risk aversion,
t : continuous time from $t = 0$ to $t = T$ on SRM-installed lane.

Equation (1) expresses how to maximize the sum of present discounted value of $U(v_{\mathrm{S}}(t) | \hat{v}_{\mathrm{S}})$ obtained at every steps on SRM-installed lane. Equation (7) determines $U(v_{\mathrm{S}}(t) | \hat{v}_{\mathrm{S}})$ in a concrete manner. The first term of equation (7) means that the speed utility increases when $v_{\mathrm{S}}(t)$ increases, so that this term indicates the comfort of driving. The second term means that the speed utility decreases when the difference between $v_{\mathrm{S}}(t)$ and $\hat{v}_{\mathrm{S}}$ increases, so that this term indicates the safety of driving. When σ increases, the driver is more likely to underestimate the speed utility at the entry of the curve. When μ increases, he is more likely to feel the risk of accidents in the situation of high speed.

Equation (2) expresses how the driver perceives $v_{\mathrm{O}}(t)$ through the visual perception of $L(t)$ affecting $v_{\mathrm{S}}(t)$, where $L(t)$ is a control variable. In this study, function f is referred to as "optic flow function". Equation (2) represents that the difference between optic flow $f(v_{\mathrm{O}}(t), L(t))$ and perceived speed $v_{\mathrm{S}}(t)$ is equivalent to the derivative of $v_{\mathrm{S}}(t)$ with respect to time t.

The optic flow is visual information that the driver can obtain while driving (Lee, 1976). Equation (4) gives the optic flow a concrete shape of f. The driver is watching the spacing pattern of SRMs flowing at relative speed against the vehicle speed. The driver can perceive the vehicle speed because of this optic flow. Parameter ξ is the effect of the spacing pattern on the visual perception.

Equation (3) expresses that $\dot{v}_{\mathrm{S}}(t)$ is proportional to $\dot{v}_{\mathrm{O}}(t)$ and proportionality coefficient α is independent from time t. Thus, equation (3) represents that there is a systematic discrepancy between $\dot{v}_{\mathrm{S}}(t)$ and $\dot{v}_{\mathrm{O}}(t)$.

Finally, equations (5) and (6) express initial condition and transversality condition, respectively (Chiang, 1992).

2.2. Risk of rear-end collision of a following vehicle

We apply a car-following model to evaluate the risk of rear-end collision of the following vehicle. Especially, we select the Kometani-Sasaki model (Kometani & Sasaki, 1958) that can describe the car-following behavior when acceleration and deceleration of the leading vehicle affect the behavior of the following vehicle. The model can be described as follows:

$$\dot{v}_{\mathrm{O}}^{\mathrm{F}}(t + T) = \beta_1 \left\{ v_{\mathrm{O}}^{\mathrm{L}}(t) - v_{\mathrm{O}}^{\mathrm{F}}(t) \right\} + \beta_2 \dot{v}_{\mathrm{O}}^{\mathrm{L}}(t), \tag{8}$$

where,
$v_{\mathrm{O}}^{\mathrm{F}}(t)$: instantaneous speed of the following vehicle at time t,
$v_{\mathrm{O}}^{\mathrm{L}}(t)$: instantaneous speed of the leading vehicle at time t,
T : time of delayed reaction,
β_1, β_2: parameters.

The first term of equation (8) indicates the effect of the difference in speeds between the leading and following vehicles on the following driver's behavior. The second term indicates the effect of the acceleration and deceleration of the leading vehicle on the following driver's behavior (Kometani & Sasaki, 1958).

In this study, we use the Possibility Index for Collision with Urgent Deceleration, PICUD (Uno, et al., 2002), which is one of the major indices regarding the rear-end collision. The unit of this index is distance. When PICUD is less than zero, the following vehicle is no longer able to avoid the rear-end collision in the situation of urgent deceleration of the leading vehicle. The value of PICUD, r_{PICUD}, can be calculated by using the following formula:

$$r_{\mathrm{PICUD}} = \frac{v_{\mathrm{O}}^{\mathrm{L}}(t)^2}{-2\phi} + \bar{s}(t) - \left\{ v_{\mathrm{O}}^{\mathrm{F}}(t)\Delta t + \frac{v_{\mathrm{O}}^{\mathrm{F}}(t)^2}{-2\phi} \right\}, \tag{9}$$

where,
ϕ : degree of urgent deceleration of the leading and following vehicles,
$\bar{s}(t)$: distance headway at time t,
Δt : time between urgent deceleration of the leading vehicle and braking of the following vehicle.

3. Solution

3.1. Solver for the optimal control problem

The Lagrangian, Φ, of the optimal control problem expressed by equations (1) to (7) can be formulated by using the Hamiltonian, H, as follows (see Appendix A):

$$\Phi = \int_0^T H[v_{\mathrm{S}}(t), v_{\mathrm{O}}(t), L(t), \lambda(t)]\mathrm{d}t + \int_0^T \dot{\lambda}(t) v_{\mathrm{S}}(t)\mathrm{d}t - \lambda(T)v_{\mathrm{S}}(T) + \lambda(0)v_{\mathrm{S}}(0) + \eta v_{\mathrm{O}}(T)\exp[-\bar{\sigma}T], \tag{10}$$

$$H[v_{\mathrm{S}}(t), v_{\mathrm{O}}(t), L(t), \lambda(t)] = U(v_{\mathrm{S}}(t)|\hat{v}_{\mathrm{S}})\exp[-\sigma t] + \lambda(t)\left\{ f\left(v_{\mathrm{O}}(t), L(t)\right) - v_{\mathrm{S}}(t) \right\}. \tag{11}$$

The first-order condition to maximize Lagrangian Φ can derive the following function (see Appendix A).

$$\dot{v}_{\mathrm{S}}(t) = \left\{ \frac{1+L(t)^{-\xi}}{\alpha} - \sigma \right\} \frac{1-\exp[\mu\{v_{\mathrm{S}}(t)-\hat{v}_{\mathrm{S}}\}]}{\mu\exp[\mu\{v_{\mathrm{S}}(t)-\hat{v}_{\mathrm{S}}\}]}. \tag{12}$$

Equation (12) describes that $\dot{v}_{\mathrm{S}}(t)$ can be determined by $L(t)$, $v_{\mathrm{S}}(t)$, $\hat{v}_{\mathrm{S}}$, ξ, α, σ and μ.

3.2. Estimating the model parameters

Equations (2), (3) and (4) can derive the following equation.

$$v_{\mathrm{S}}(t) = \left\{1 + L(t)^{-\xi}\right\} v_{\mathrm{O}}(t) - \alpha\dot{v}_{\mathrm{O}}(t). \tag{13}$$

By substituting equation (13) into equation (12), the following equation can be derived.

$$1 + L(t)^{-\xi} - \alpha \cdot \left\{ \sigma + \frac{\mu\alpha v_{\mathrm{O}}(t)\exp\left[\mu\left\{\left\{1+L(t)^{-\xi}\right\}v_{\mathrm{O}}(t) - \alpha\dot{v}_{\mathrm{O}}(t) - \hat{v}_{\mathrm{S}}\right\}\right]}{1-\exp\left[\mu\left\{\left\{1+L(t)^{-\xi}\right\}v_{\mathrm{O}}(t) - \alpha\dot{v}_{\mathrm{O}}(t) - \hat{v}_{\mathrm{S}}\right\}\right]} \right\} = 0. \tag{14}$$

Now, we define error function Ψ that is normally distributed with mean 0 and variance ρ, as follows:

$$\Psi[\alpha,\xi|v_{\mathrm{O}}(t),L(t);\hat{v}_{\mathrm{S}},\mu,\sigma]=1+L(t)^{-\xi}-\alpha\cdot\left\{\sigma+\frac{\mu\alpha v_{\mathrm{O}}(t)\exp\left[\mu\left\{\{1+L(t)^{-\xi}\}v_{\mathrm{O}}(t)-\alpha\dot{v}_{\mathrm{O}}(t)-\hat{v}_{\mathrm{S}}\right\}\right]}{1-\exp\left[\mu\left\{\{1+L(t)^{-\xi}\}v_{\mathrm{O}}(t)-\alpha\dot{v}_{\mathrm{O}}(t)-\hat{v}_{\mathrm{S}}\right\}\right]}\right\}. \tag{15}$$

Accordingly, likelihood function $\mathcal{L}$ can be defined as follows:

$$\mathcal{L}(\alpha,\xi|v_{\mathrm{O}}(t),L(t);\hat{v}_{\mathrm{S}},\mu,\sigma,\rho)=\prod_{t=0}^{T}\frac{1}{\sqrt{2\pi}\rho}\exp\left[-\frac{\Psi[\alpha,\xi|v_{\mathrm{O}}(t),L(t);\hat{v}_{\mathrm{S}},\mu,\sigma]^2}{2\rho^2}\right]. \tag{16}$$

The log-likelihood function of equation (16) becomes a multiple peak function that is overlapping many convex upward functions. Thus, when we estimate parameters maximizing this log-likelihood function, we cannot derive an unique solution from the Newton-Raphson method, because of convergence at a local solution. Therefore, we use the Markov Chain Monte Carlo (MCMC) method based on the Metropolis-Hastings algorithm (Chib & Greenberg, 1995), in order to estimate the parameters to converge at a global solution.

4. Simulation data

4.1. Input data and constant parameters

Because of simulation difficulty, we must set several parameters of the models as constant parameters. For the model of the perception and behavior of the leading driver, we set the discount rate of time preference, σ, the degree of risk aversion, μ, and the speed at the initial time, $\bar{v}_{\mathrm{O}}\equiv v_{\mathrm{O}}^{\mathrm{L}}(0)$, as constant parameters. For the model of the car-following behavior of the following vehicle, we set the time of delayed reaction, T, and the coefficients, β_1,β_2, as constant parameters. For the model of the rear-end collision risk, we set the degree of deceleration, ϕ, and the time between urgent deceleration of the leading vehicle and braking of the following vehicle, Δt, as constant parameters. Under the assumption that σ and μ are given, we estimate parameters α and ξ by using input data regarding $v_{\mathrm{O}}(t)$, $\dot{v}_{\mathrm{O}}(t)$ and $L(t)$. In this study, we obtain the data from a driving simulation experiment that we have already been conducted in our previous study (Yotsutsuji, 2017).

4.2. The experiment

To define a few key terms in this study, let us shortly explain the contents of the driving simulation experiment in our previous study.

In the experiment, we employed a fixed-base driving simulator using software named UC-win/Road Driving Sim, which can display at a rate of 120 frames per second. The total width of the roadway was 13 m, comprising two 3.5 m lanes, a 1.5 m median strip, two 1.75 m left shoulders, and two 0.5 m right shoulders. The width of each transverse marking line of SRMs was 45 cm. The curve radius was varied between 200 m and 1,000 m in increments of 100 m. In this study, especially, we focus on the curve radius of 200 m as a sharp bend.

A lane equipped with SRMs was longitudinally divided into several ranges, which is referred to as “section”. The spacing pattern was dealt with as the spatial arrangement of the transverse marking lines on SRM-installed lane, where the spacing was equal within an arbitrary section and decreasing between two adjacent sections toward the curve. The “decrease ratio (DR)” of the spacing length between two adjacent sections was defined as an index that was calculated by dividing the difference between the “spacing length in the forward section” and the “spacing length in the backward section” by the “spacing length in the backward section”. Thus, in this study, the problem of adjusting the spacing pattern according to a change in the curve radius is replaced by that of finding the optimal location of the greatest DR section in accordance with the change in the curve radius.

In the experiment, 20 people were openly recruited as participants, including 10 elderly people aged 65 years or older. During the experiment, although the speedometer was displayed on screen in 100 m of the first section in SRM-installed lane, it was not displayed in the remaining sections. An experimenter instructed each of participants to accelerate to 80 km/h until passing the first section, and to keep their driving speed at 80 km/h as constant as possible

Table 1. Configuration of spacing pattern of SRMs (Yotsutsuji, 2017)

Pattern	Greater DR section	Section name Length [m]	Z 100	I 100	II 100	III 100	IV 100	V 100
A	Constant	Spacing [m]	12.00	12.00	12.00	12.00	12.00	12.00
		DR [%]	0	0	0	0	0	0
B	Beginning	Spacing [m]	12.00	10.29	9.18	8.72	8.28	7.87
		DR [%]	0	15	10	5	5	5
C	Middle	Spacing [m]	12.00	11.40	10.26	8.72	7.85	7.46
		DR [%]	0	5	10	15	10	5
D	End	Spacing [m]	12.00	11.40	10.83	10.29	9.26	7.87
		DR [%]	0	5	5	5	10	15

in the remaining sections without watching the speedometer, and to pass the curve safely by decelerating as necessary.

Table 1 shows the four spacing patterns labelled A, B, C and D, on which we focus in this study. Pattern A has a DR of zero in all sections and is used as a baseline. Patterns B, C and D have higher DRs in the beginning, middle and end sections, respectively, compared with the remaining sections. The driver run in sections Z to V toward the curve.

5. Simulation results

5.1. Numerical example of the leading driver's behavior

Figure 1 shows a numerical example regarding the behavior of the leading driver with $\sigma = 0.5$ and $\mu = 0.3$ in the case of the curve radius of 200 m, corresponding to the four spacing patterns.

In Figure 1, horizontal axis indicates travel distance to the transition curve section, where the origin denotes the beginning location of section Z and the right hand of the axis is toward the curve. Longitudinal axis indicates the actual speed, $v_{\mathrm{O}}(t)$, the perceived speed, $v_{\mathrm{S}}(t)$, and the maximum safe speed, $\hat{v}_{\mathrm{S}}$. The value just located on the longitudinal axis corresponding to the origin represents the initial speed at $t = 0$.

In Figure 1, the values of $v_{\mathrm{O}}(0)$ are equivalent among the four spacing patterns, and each of them is numerically equal to $v_{\mathrm{S}}(0)$. In addition, $v_{\mathrm{O}}(0)$, $v_{\mathrm{S}}(0)$, and $\hat{v}_{\mathrm{S}}$ are set as 27.8 m/s (100 km/h), 27.8 m/s (100 km/h), and 16.7 m/s (60 km/h), respectively. With regard to the curve radius corresponding to a design speed of 60 km/h, a desired minimum curve radius is recommended as 200 m (JRA, 2004). In Figure 1, it is assumed that $\hat{v}_{\mathrm{S}}$ is equal to $\hat{v}_{\mathrm{O}}$, and that the value of it is 16.7 m/s (60 km/h) which is corresponding to the desired minimum curve radius of 200 m.

The example described in Figure 1 shows the following results: 1) In the case of pattern A, both $v_{\mathrm{O}}(T)$ and $v_{\mathrm{S}}(T)$ have exceeded $\hat{v}_{\mathrm{O}}$ in the end of section V. 2) In the cases of patterns B and C, although $v_{\mathrm{O}}(T)$ has exceeded $\hat{v}_{\mathrm{O}}$ in the end of section V, the value of $v_{\mathrm{S}}(t)$ has dipped below $\hat{v}_{\mathrm{O}}$ before the end of section V. 3) In the case of pattern D, both values of $v_{\mathrm{O}}(t)$ and $v_{\mathrm{S}}(t)$ have dipped below $\hat{v}_{\mathrm{O}}$ before the end of section V.

5.2. Numerical example of the rear-end collision risk

Figure 2 shows a numerical example regarding the rear-end collision risk which represents that the following vehicle may collide with the leading vehicle operated by the driver with $\sigma = 0.5$ and $\mu = 0.3$ in the case of the curve radius of 200 m.

In Figure 2, horizontal axis indicates travel time to the transition curve section, where the origin denotes the beginning location of section Z and the right hand of the axis is toward the curve. Longitudinal axis indicates the values of PICUD.

For the parameters of PICUD, ϕ and Δt are set as –3.0 m/s^2 and 1.25 s, respectively. For the parameters of the car-following model, β_1, β_2, T and $\mathrm{v}_0^{\mathrm{F}}(0)$ are set as 0.3, 0.3, 1.25 s and 28.0 m/s, respectively. As the results, the values of PICUD are 14.1 m, 3.0 m, 7.1 m and 0.3 m in the end of section V under patterns A, B, C and D, respectively.

The example described in Figure 2 shows the following results: 1) Patterns A, B and C seems to be at little risk of the rear-end collision. 2) Pattern D may produce a high risk of the rear-end collision of the following vehicle before the leading vehicle enters the curve.

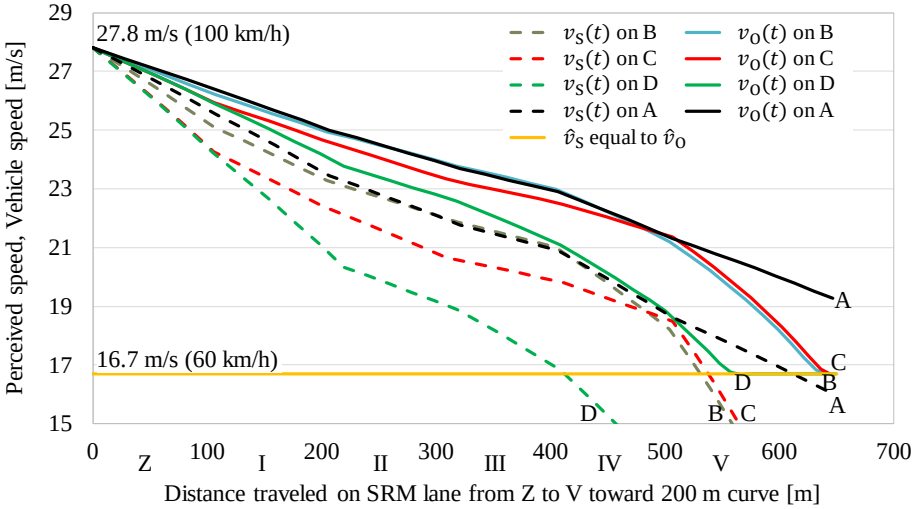

Figure 1. Trajectories of the vehicle speed and the perceived speed based on the simulation

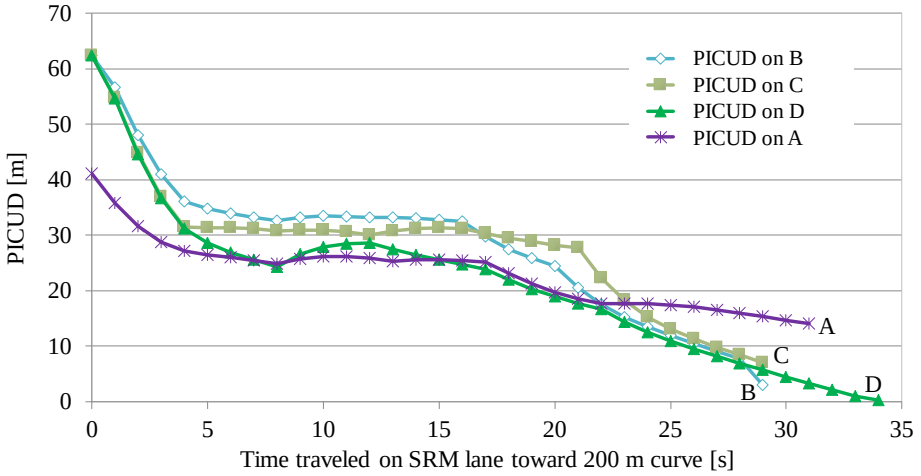

Figure 2. Trajectories of the rear-end collision risk based on the simulation

6. Discussion

The numerical examples shown in Figures 1 and 2 correspond to the case that there is a sharp bend after SRM-installed lane, and the leading driver begins to travel with high speed at the initial time, and also he has the risk of rear-end collision of the following vehicle before entering the curve. In this case, our numerical examples have shown the results as follows:

- There is the case that the spacing pattern of SRMs with greater DR in the end section than in the remaining sections may produce a high risk of the rear-end collision of the following vehicle before the leading vehicle enters the curve, although the leading vehicle can safely enters the curve.
- There is the case that the spacing pattern of SRMs with DRs of zero in all sections may produce an accident with which the leading vehicle meets within the curve, although the rear-end collision risk of the following vehicle is very few.

In each of the four spacing patterns, as the leading driver is approaching the curve, a discrepancy between the perceived speed and the vehicle speed increases progressively with the decreasing distance from the curve. At the same time, trajectories of the discrepancy are different among the four spacing patterns. It is considered that one of the reasons why this phenomenon gives rise to is that, when the leading driver plans to decelerate in order to drop the perceived speed down below the maximum safe speed at the timing of the curve entry, the spacing pattern of SRMs can hasten or delay the timing of such drop-down situation. We can see this because Figure 1 shows that the drop-down points are the point near 400 m for pattern D, the point near 550 m for patterns B and C, and the point over 600 m for pattern A. In addition, even though the timing of the drop-down situation with respect to the perceived speed can be hastened, the vehicle speed is not always dropped down below the maximum safe speed before the curve entry. We can see this because Figure 1 shows that the discrepancy in speeds between patterns B and C remains at the point of 600 m, although the perceived speed has already been dropped down at the point near 550 m.

7. Conclusion

In this study, we numerically simulated both the optimal speed trajectory of the leading vehicle that moved on SRM-installed lane toward the curve and the risk of rear-end collision of the following vehicle before the leading vehicle entered the curve, and we examined the optimal spacing pattern of SRMs affecting the leading driver's speed choice before the curve entry. We constructed the optimal control model that described the driving behavior with the speed perception, and we estimated the rear-end collision risk by using PICUD. Our simulation results showed that the optimization of the spacing pattern of SRMs had to consider not only the optimal speed trajectory of the leading vehicle but also the rear-end collision risk of the following vehicle.

There remains some topics that should be explored in the future works. Regarding the speed utility function, we assumed that, without any explanation, both the perceived speed and the degree of risk aversion independently affected the speed utility. The relationship between speed perception and risk aversion must explain to be clear. Regarding the rear-end collision risk, we dealt with only two vehicles. Analyzing the effect of SRMs on adjustment of platoon speed will be required. Furthermore, regarding the simulation study, we will have to verify whether or not the spacing pattern of SRMs needs to vary according to the curve radius, through empirical study based on causal inference.

Acknowledgements

This study was carried out during first-author's previous employment at Kobe University, by using data from a driving simulation experiment financially supported by a collaborative research project between Kobe University and NEXCO RI. This study received financial support from JSPS Grant-in-Aid for Scientific Research (B) No. 16H03017. The authors express our gratitude for constructive suggestions for MCMC estimation from Prof. Takamasa Iyo, and thank to Mr. Kazuki Kitamura who did several calculations as part of his graduation work at Kobe University.

Appendix A. Solution of the optimal control problem expressed by equations (1) to (7)

The Lagrangian, Φ, is defined as follows:

$$\Phi = \int_0^T U(v_S(t)|\hat{v}_S)\exp[-\sigma t]\,\mathrm{d}t + \int_0^T \lambda(t)\{f(v_O(t), L(t)) - v_S(t) - \alpha\dot{v}_O(t)\}\mathrm{d}t + \eta v_O(T)\exp[-\bar{\sigma}T]. \quad \text{(A1)}$$

To derive the Hamiltonian, we prepare the derivative of $\lambda(t)v_S(t)$ and $\alpha\lambda(t)v_O(t)$, as follows:

$$\frac{\mathrm{d}}{\mathrm{d}t}[\lambda(t)v_S(t)] = \dot{\lambda}(t)v_S(t) + \lambda(t)\dot{v}_S(t) = \dot{\lambda}(t)v_S(t) + \alpha\lambda(t)\dot{v}_O(t), \quad \text{(A2)}$$

$$\frac{\mathrm{d}}{\mathrm{d}t}[\alpha\lambda(t)v_O(t)] = \alpha\dot{\lambda}(t)v_O(t) + \alpha\lambda(t)\dot{v}_O(t). \quad \text{(A3)}$$

By integrating both side of each of equations (A2) and (A3), we obtain the following equations.

$$\int_0^T \alpha\lambda(t)\dot{v}_{\mathrm{O}}(t)\mathrm{d}t = \int_0^T \frac{\mathrm{d}}{\mathrm{d}t}[\lambda(t)v_{\mathrm{S}}(t)]\mathrm{d}t - \int_0^T \dot{\lambda}(t)v_{\mathrm{S}}(t)\mathrm{d}t = \lambda(T)v_{\mathrm{S}}(T) - \lambda(0)v_{\mathrm{S}}(0) - \int_0^T \dot{\lambda}(t)v_{\mathrm{S}}(t)\mathrm{d}t, \quad \text{(A4)}$$

$$\int_0^T \alpha\lambda(t)\dot{v}_{\mathrm{O}}(t)\mathrm{d}t = \int_0^T \frac{\mathrm{d}}{\mathrm{d}t}[\alpha\lambda(t)v_{\mathrm{O}}(t)]\mathrm{d}t - \int_0^T \alpha\dot{\lambda}(t)v_{\mathrm{O}}(t)\mathrm{d}t. \quad \text{(A5)}$$

By substituting equation (A4) into equation (A1), we obtain equations (11) and (12). Now, the first-order conditions with respect to $v_{\mathrm{S}}(t)$, $v_{\mathrm{O}}(t)$ and $\lambda(t)$ are derived from Lagrangian Φ, as follows:

$$\frac{\mathrm{d}}{\mathrm{d}v_{\mathrm{S}}} U(v_{\mathrm{S}}(t)|\hat{v}_{\mathrm{S}}) \exp[-\sigma t] - \lambda(t) = U'(v_{\mathrm{S}}(t)|\hat{v}_{\mathrm{S}}) \exp[-\sigma t] - \lambda(t) = 0, \quad \text{(A6)}$$

$$\lambda(t) \frac{\mathrm{d}}{\mathrm{d}v_{\mathrm{O}}} f\big(v_{\mathrm{O}}(t), L(t)\big) + \alpha\dot{\lambda}(t) = 0, \quad \text{(A7)}$$

$$f(v_{\mathrm{O}}(t), L(t)) = v_{\mathrm{S}}(t) + \dot{v}_{\mathrm{S}}(t). \quad \text{(A8)}$$

By differentiating equation (A6) with respect to t, we obtain the following equation.

$$\dot{\lambda}(t) = -\sigma U'(v_{\mathrm{S}}(t)|\hat{v}_{\mathrm{S}}) \exp[-\sigma t] + U''(v_{\mathrm{S}}(t)|\hat{v}_{\mathrm{S}})\dot{v}_{\mathrm{S}}(t) \exp[-\sigma t]. \quad \text{(A9)}$$

By substituting equation (A9) into equation (A7), we obtain the following equation.

$$\frac{\mathrm{d}}{\mathrm{d}v_{\mathrm{O}}} f\big(v_{\mathrm{O}}(t), L(t)\big) = \alpha\left\{\sigma - \frac{U''\big(v_{\mathrm{S}}(t)\big|\hat{v}_{\mathrm{S}}\big)\dot{v}_{\mathrm{S}}(t)}{U'\big(v_{\mathrm{S}}(t)\big|\hat{v}_{\mathrm{S}}\big)}\right\}. \quad \text{(A10)}$$

Finally, by substituting the derivative of equation (4) with respect to $v_{\mathrm{O}}(t)$ into equation (A10), we obtain the following equation.

$$1 + L(t)^{-\xi} = \alpha\left\{\sigma - \frac{U''\big(v_{\mathrm{S}}(t)\big|\hat{v}_{\mathrm{S}}\big)\dot{v}_{\mathrm{S}}(t)}{U'\big(v_{\mathrm{S}}(t)\big|\hat{v}_{\mathrm{S}}\big)}\right\}. \quad \text{(A11)}$$

By substituting the derivative of equation (7) with respect to $v_{\mathrm{S}}(t)$ into equation (A11), we obtain equation (12).

References

Chiang, A. C. 1992. Elements of dynamic optimization. McGaw-Hill.

Chib, S., Greenberg, E. 1995. Understanding the Metropolis-Hastings algorithm. The American Statistician 49.4, 327-335.

Federal Highway Administration 2009. Speed reduction markings. Manual on Uniform Traffic Control Devices (MUTCD) 3B.22, 393-394.

Hayward, J. C. 1972. Near-miss determination through use of a scale of danger. Highway Research Record 384, 24-34.

Japan Road Association 2004. Explanation and Application of Road Structure Ordinance. Maruzen, 309-320.

Kometani, E., Sasaki, T. 1958. On the stability of traffic flow (Report-I). Journal of Operational Research 2.1, 11-16.

Lee, D. N. 1976. A theory of visual control of braking based on information about time-to-collision. Perception 5.4, 437-459.

Uno, N., Iida, Y., Itsubo, S., Yasuhara, S. 2002. A microscopic analysis of traffic conflict caused by lane-changing vehicle at weaving section. In Proceedings of the 13th Mini-EURO Conference-Handling Uncertainty in the Analysis of Traffic and Transportation Systems, Bari, Italy.

Yotsutsuji, H. (2017). Does array pattern of speed reduction markings need to be changed in accordance with horizontal curve radius?: causality analysis using driving simulator data. Journal of the Eastern Asia Society for Transportation Studies 12, 1904-1916.